# Combined Genetic and Metabolic Manipulation of Lipids in Rhodobacter sphaeroides Reveals Non−Phospholipid Substitutions in Fully Active Cytochrome c Oxidase

**ARTICLE** *in* BIOCHEMISTRY · MAY 2011

Impact Factor: 3.02 · DOI: 10.1021/bi1017039 · Source: PubMed



**6 AUTHORS**, INCLUDING:

Gavin E Reid
University of Melbourne
**150** PUBLICATIONS **6,711** CITATIONS
SEE PROFILE

Shelagh Ferguson-Miller
Michigan State University
**147** PUBLICATIONS **7,239** CITATIONS
SEE PROFILE

Published in final edited form as:
*Biochemistry*. 2011 May 17; 50(19): 3891–3902. doi:10.1021/bi1017039.

# Combined Genetic and Metabolic Manipulation of Lipids in *Rhodobacter sphaeroides* Reveals Non-Phospholipid Substitutions in Fully Active Cytochrome *c* Oxidase†

**Xi Zhang**[1,2], **Carrie Hiser**[1], **Banita Tamot**[1], **Christoph Benning**[1], **Gavin E. Reid**[1,2], and **Shelagh M. Ferguson-Miller**[1,*]

[1] Department of Biochemistry and Molecular Biology, Michigan State University, East Lansing, MI 48824

[2] Department of Chemistry, Michigan State University, East Lansing, MI 48824

## Abstract

A specific requirement for lipids, particularly cardiolipin (CL), in cytochrome *c* oxidase (C*c*O) has been reported in many previous studies using mainly *in vitro* lipid removal approaches in mammalian systems. Our accompanying paper shows that C*c*O produced in markedly CL-depleted *Rhodobacter sphaeroides* displays wild type properties in all respects, likely enabled by quantitative substitution by other negatively charged lipids. To further examine the structural basis for the lipid requirements of *R. sphaeroides* C*c*O and the extent of interchangeability between lipids, a metabolic approach was employed to enhance the alteration of the lipid profiles of the C*c*O-expressing strains of *R. sphaeroides in vivo* using a phosphate-limiting growth medium in addition to the CL-deficient mutation. Strikingly, the purified CcO produced under these conditions still maintained wild type function and characteristics, in spite of even greater depletion of cardiolipin compared to the CL-deficient mutant alone (undetectable by MS) and drastically altered profiles of all the phospholipids and non-phospholipids. The lipids in the membrane and in the purified C*c*O were identified and quantified by ESI and MALDI mass spectrometry and tandem mass spectrometry. Comparison between the molecular structures of those lipids that showed major changes provide new insight into the structural rationale for the flexible lipid requirements of C*c*O from *R. sphaeroides*, and reveal a more comprehensive interchangeability network between different phospholipids and non-phospholipids.

Lipid biosynthesis in bacteria is highly sensitive and adaptable to the growth medium (1). In addition to modification by genetic mutations as described earlier (accompanying paper), the lipid profile of bacteria can be modulated through metabolic approaches such as using low-phosphate growth media (1–4). Since limited phosphate in the growth medium affects all types of phosphate-containing lipids, this approach can be used as another tool to evaluate the functional significance of phospholipids and of non-phospholipids *in vivo*, with respect to bacterial growth and the properties of well-characterized membrane proteins. Previous studies of both *R. sphaeroides* (1) and *Sinorhizobium melitoti* (3, 4) found that these bacteria are viable at phosphate concentrations as low as 0.1 mM (compared to the normal 20 mM (1)), but phosphate-limiting media significantly change the membrane lipid profile. The

†The work was supported by NIH R01 GM26916 (SFM) and the Michigan State University Center of Excellence for the Structural Analysis of Membrane Proteins (CB, GER and SFM).

*Corresponding author: Shelagh M. Ferguson-Miller, Ph.D., Department of Biochemistry and Molecular Biology, Michigan State University, East Lansing, MI 48824, Phone: (517) 353-3512, Fax: (517) 353-9334, fergus20@msu.edu.

amounts of phospholipids are found to be significantly reduced, and novel types of phosphate-free lipids are produced in high abundance (1).

Previous lipid biochemistry studies found that when grown in media containing abundant phosphate (5, 6), the membranes of the wild type *R. sphaeroides* strain 2.4.1 contain phosphatidylethanolamine (PE), phosphatidylcholine (PC), phosphatidylglycerol (PG) and cardiolipin (CL), and the non-phospholipids such as sulfoquinovosyldiacylglyceride (SQDG) and ornithine lipids (OL), but phospholipids are the predominant components. Under phosphate-limiting growth conditions, the novel non-phosphate-containing glycolipids glucosylgalactosyldiacylglyceride (GGDG) and diacylglyceryl-N, N, N-trimethylhomoserine (DGTS) were produced, and the production of SQDG and OL was increased (1). DGTS was proposed to functionally compensate for PC, SQDG for PG, and OL for PE, based on the similarity of the charge state in the head group (1, 2, 7). DGTS was also the predominant type of lipids in *Sinorhizobium melitoti* under phosphate-limiting growth (3).

Mutations in genes involved in lipid synthesis can cause a specific deficiency in a particular type of lipid, such as PC, CL or SQDG, but the amount of some other types of lipids was often seen to increase as well, interpreted as a compensatory mechanism to fulfill the required biological functions (5). Cardiolipin-deficiency, which is often created by mutating the cardiolipin synthase (8, 9), produced an increased level of PG lipids (9). Therefore it is proposed that the high structural resemblance of PG to CL makes PG the essential lipid that can functionally replace CL. On the other hand, SQDG and PG lipids appear to be inter-changeable in *R. sphaeroides* because both have negative charge in the head group, and the depletion of both SQDG and PG is lethal (2). An effect of PE-depletion on some membrane proteins can be restored by monoglucosyldiacyl-glycerol due to similarity in the molecular shape (10).

One question raised from comparing these previous findings is, are such types of functional compatibility determined more by the phosphatidylglyceride backbone structure, by the negative or positive charge state, by the head group functional groups, or by the molecular shape? Since phosphate-limited growth can decrease the production of the entire set of phospholipids, and increase the relative amount of polar non-phospholipids, its combination with the genetically produced specific lipid-deficiency should be able to provide deeper insights into the functional substitutability between different types of lipids, and therefore a better understanding of the essentiality of a particular type of lipid, such as cardiolipin.

In this study, a cardiolipin-abundant wild type strain and a cardiolipin-deficient strain of *R. sphaeroides* were grown in normal-phosphate and low-phosphate media and compared with respect to growth, membrane lipid profiles and cytochrome *c* oxidase (C*c*O) expression levels. The C*c*O was purified from these two different strains under two different growth conditions and characterized by UV-Vis spectroscopic properties, subunit-composition and enzymatic activity. The lipid profiles of the membranes and the purified enzymes were analyzed by using quantitative ESI and MALDI MS and MS/MS, to relate the observed spectral and functional properties of C*c*O and *R. sphaeroides* to the lipid composition. The results show a striking resilience of C*c*O to dramatic changes in its lipid environment.

## Materials and Methods

### Media and growth conditions

The cardiolipin-abundant wild type strain, 169–2.4.1 (WT) and the CL-deficient mutant strain 169CL3 (CL−) were grown in parallel in both phosphate-abundant (P+) and phosphate-limiting (P−) conditions. The normal-phosphate conditions were: Sistrom's

succinate-basal salts medium with $KH_2PO_4$ concentration of 20 mM (pH 7.0) and appropriate antibiotics as described previously (11, 12). The cells were grown on agar-solidified medium or in liquid cultures at 30 °C under aerobic chemoheterotrophic conditions described in (13). For the phosphate-limiting growth, the 20 mM $KH_2PO_4$ in the Sistrom's media was replaced with 50 mM HEPES-KOH and 0.1 mM $KH_2PO_4$ (pH 6.8). Strain designations: WT/ P+, 169–2.4.1 grown under normal phosphate; CL−/ P+, 169CL3 under normal phosphate; WT/ P−, 169–2.4.1 under low phosphate; and CL−/ P−, 169CL3 under low phosphate.

### Isolation of R. sphaeroides cell membrane pellets and CcO purification

The C*c*O over-expressed in all *R. sphaeroides* strains (Table S1) contained a 6x histidine tag at the C-terminus of subunit II. *R. sphaeroides* cells were harvested by centrifugation in a GS-3 rotor at 14,000 g for 20 minutes and resuspended in pH 6.5 buffer containing 50 mM $KH_2PO_4$, or 50 mM Bis-Tris propane for cells grown under phosphate-limiting conditions and 1 mM EDTA. Further processing was carried out as previously described (13). A typical yield obtained from fifteen 2.8 L Fernbach flasks of WT or CL− cell cultures was approximately 40 mg C*c*O; in high phosphate (P+) and in low phosphate (P−) conditions the yields were similar. *R. sphaeroides* C*c*O was purified from isolated membrane pellets as described previously (14).

### UV-Visible spectroscopy of membrane suspension and purified CcO

UV-Visible optical spectra were recorded on a Perkin-Elmer Lambda 40P UV-visible spectrophotometer. For the crude membrane samples, dithionite-reduced minus ferricyanide-oxidized spectra were collected from 500 to 700 nm wavelengths and the level of C*c*O was quantified by using the extinction coefficient $\Delta\varepsilon_{606-630} = 24\ cm^{-1}mM^{-1}$ (13). For the purified C*c*O samples, an absolute spectrum was measured with and without reduction with sodium dithionite from 250 to 700 nm, and the level of C*c*O was quantified by using the extinction coefficient $\Delta\varepsilon_{606-640} = 40\ cm^{-1}mM^{-1}$ (13). To counteract the acidity of the reducing agent, the samples were diluted with buffer containing 1 mM EDTA, 0.1% (m/v) dodecyl maltoside and 100 mM HEPES pH 7.4 prior to the analysis. At least triplicate spectra were collected for each sample.

### Urea SDS-PAGE gel electrophoresis and steady state activity assay of CcO

Sodium dodecyl sulfate polyacrylamide gel electrophoresis (SDS-PAGE) was carried out as previously described (15). The steady state activity of C*c*O was measured by oxygen consumption as previously described (16), under conditions given in the figure legend.

### Extraction of lipids from isolated membranes

Triplicates of 20 μL of the resuspended membranes from *R. sphaeroides* cells (diluted with water to 1 mg/mL protein concentration determined by BCA assay) were freeze-dried, and lipids were extracted by sequential addition of 2 x 50 μL chloroform: methanol (2:1, v/v), 1 x 50 μL ethyl ether: methanol (1:1, v/v), and 2 x 50 μL chloroform: methanol: ammonium hydroxide (100:50:2, v/v/v) followed by vigorous vortexing (17). The extracts were combined, dried under vacuum and re-dissolved in 50 μL chloroform: methanol (1:1, v/v) prior to mass spectrometry analysis.

### Identification of lipids by using ESI MS and CID $MS^n$

Mass spectrometric analyses of lipids were performed using a linear quadrupole ion trap (Thermo Fisher Scientific model LTQ, San Jose, CA), equipped with a nanoelectrospray ionization source (ESI) for analysis of membrane lipid extracts, and a Thermo model LTQ-XL linear ion trap mass spectrometer equipped with vacuum matrix-assisted laser

desorption /ionization source (vMALDI) for direct analysis of membranes and purified enzymes. The total lipid extracts obtained from above were diluted 4 fold using $CHCl_3$:$CH_3OH$ (1:1, v/v) containing 40 mM ammonium hydroxide, and introduced to the mass spectrometer by direct infusion through non-coated silica tips with internal diameters of 30 μm (New Objective, Inc. Woburn, MA), at a flow rate of 0.5 μL/min. NanoESI conditions were optimized to maximize the sensitivity and stability of the precursor ions of interest while minimizing 'in-source' fragmentation. Typical nanoESI conditions were: heated capillary temperature 180 °C, spray voltage 1.8 kV, capillary voltage 20 V (−20 V for negative ion mode) and tube lens voltage 75 V (−75 V for negative ion mode). Mass spectra (MS) were acquired from m/z 150 to 2000 using enhanced scan mode.

Collision-induced dissociation (CID) tandem mass spectrometry (MS/MS) and multistage tandem mass spectrometry ($MS^n$) experiments were performed by using helium as the collision gas and an activation time of 30 ms in the linear ion trap. Collision energies were optimized for each precursor ion of interest. Typically, an activation q value of 0.2 was used in order to achieve a reasonable low-mass-cutoff while still maintaining good sensitivity. Depending on the activation q values, the corresponding optimal normalized collision energies applied were typically 25% for the phospholipids, ornithine lipids and glutamine lipids, and increased to 40% for SQDG lipids. The isolation width to obtain isotopical isolation of precursor ions was typically 1.2 Da for protonated and deprotonated ions, and 1.5–2.0 Da for non-covalent cationic or anionic adduct ions (18). The spectra shown were typically the average of 50–300 scans. Each scan was typically an average of three microscans. The target number was set at 1e4 for MS and 3e4 for $MS^n$. For the identification analysis, the maximum injection time was typically set at 50 ms for both MS and $MS^n$. For comprehensive lipid identifications, lipid precursor ions with normalized relative abundances higher than 1% in MS were further examined by MS/MS and $MS^n$ both manually and in automatic acquisition mode. The structures of lipids were determined by comparing the MS/MS and $MS^n$ spectra with those of available standards, or by rationalizing based on knowledge of the gas-phase fragmentation behaviors of lipid (1, 19–21).

### Quantification of lipids using ESI MS and CID MS/MS

Total lipid extracts from each membrane sample were diluted by 4 fold using $CHCl_3$:$CH_3OH$ (1:1, v/v) containing ammonium hydroxide at a final concentration of 40 mM, and mixed with internal standards PE 14:0/14:0, PG 14:0/14:0, PC 14:0/14:0, $CL(14:0)_4$ at final concentrations of 4 μM, 2 μM, 2 μM and 1 μM, respectively, followed by sample infusion for ESI analysis. At least triplicate independent extractions were performed, and each MS spectrum was an average of 100–250 scans, each containing 3 micro-scans, acquired from m/z 150 to 2000 in both positive and negative ion modes. The MS spectra were processed by Gaussian 5 point smoothing, and corrected for chemical base line noise, isotopic distributions and isotopic overlapping. Intensities of all the ions in the processed spectra of each sample were first normalized to the internal standards observed in MS, and then converted into the quantity (for phospholipids with available standards) or relative quantity (lipids without standards of the same head group) of each lipid species using independently generated external calibration curves (21).

Extensive MS/MS quantification experiments of lipid extracts were carried out using automatic acquisition. For all the peaks with normalized relative abundance in MS higher than 10% in the m/z range 600–1600, MS/MS spectra of isotopically isolated precursor ions (isolation width 1.2 Da for singly charged ions and 0.8 Da for doubly charged ions) were collected with 50 ms maximum injection times and under an MS/MS target number of 3e4 and an activation q value of 0.2. For all the peaks above 1% but equal to or below 10% as well as all the internal standards again, the maximum injection time was increased to 100

ms, and the number of scans collected was increased to about four fold higher than those at > 10% relative abundance whenever possible. Each scan was the average of three microscans. The normalized collision energy applied was 30% for positive ion mode and 25% for negative ion mode. Isolation and MS/MS activation of singly charged CL precursor ions using isolation widths of 10 Da were acquired using automatic acquisition, and the characteristic product ions at m/z 699 for $CL(18:1)_4$ and m/z 591 for the internal standard $CL(14:0)_4$) were used for CL quantification. MS/MS of all the SQDG species using normalized collision energies of 35% were also acquired automatically using a maximum injection time of 100 ms, regardless of the abundance in the MS spectra. These experiments were all performed on triplicate extraction samples. Quantification was based on the relative abundance ratios of primary product ions from each lipid over the lipid internal standards.

### Direct lipid identification using MALDI-LIT MS and $MS^n$

Direct MS and $MS^n$ analyses of isolated membranes and purified C*c*O were performed on vMALDI-LIT. One μL of either resuspended membrane (at a protein concentration of 0.25 mg/mL determined by the BCA assay using bovine serum albumin as the standard) or 1 μL of purified C*c*O (25 μM), was applied to individual spots on the stainless steel MALDI sample plate and dried in air, followed by application of 1 μL of 0.1 M (for membrane samples) or 0.5 M (for purified enzymes) 2, 5-hydroxy benzoic acid (2, 5-DHB) dissolved in acetonitrile: water (2:1, v/v). MS and MS/MS spectra were acquired in negative and positive ion modes using enhanced resonance ejection scan conditions. Typical optimal laser power setting was 20 for positive ion mode analyses and 30 for negative ion mode analyses. MS was acquired for m/z 200–2000. CID MS/MS and $MS^n$ spectra were acquired at a normalized collision energy of 30%, isolation widths of 1.2 or 1.5 Da to achieve isotopical isolation, and an activation q of 0.2. The MALDI spectra shown were the average of 250 scans. The MALDI MS spectra were processed by Gaussian 5 point smoothing and corrected for chemical base line noise prior to relative quantification of CL by using MS peak heights.

### Direct relative quantitative lipid analysis using MALDI-LIT MS

An internal standard mixture containing PE 14:0/14:0, PG 14:0/14:0, PC 14:0/14:0 and $CL(14:0)_4$ at final concentrations of 10 μM, 5 μM, 1.25 μM and 1.25 μM, respectively, in methanol was added to the membrane suspension (0.25 mg/mL final protein concentration), or the purified C*c*O solution (4.2 μM final C*c*O concentration, i.e. 0.5 mg/mL protein concentration) to form one-phase mixtures. One μL of each mixture was then applied to the vMALDI plate, and processed as described above.

## Results and Discussion

### Cell growth, CcO production and purification stability

No obvious difference in the cell culture optical density at harvest was observed between the WT and CL− strains grown under phosphate-abundant or phosphate-deficient conditions. The UV-Vis spectroscopic analysis of the isolated membranes also show very similar spectral characteristics for all of these four samples and no shift in the absorption peak at 606 nm (heme a) was observed (Figure 1A). These findings indicate that all four conditions can produce similar amounts of C*c*O, and that the C*c*O produced has native structure in the membrane, as indicated by the unaltered spectral characteristics, even when both CL deficiency and phosphate deficiency is imposed. The purification profiles of C*c*O from Ni-NTA FPLC are also very similar for these four samples, in term of the peak elution conditions, the relative abundances of the eluted protein peaks (data not shown) and the purification yields. It appears that neither the CL deficiency nor phosphate deficiency, nor

the combination affects the production, the metal center assembly, or the stability of the multi-subunit protein complex during enzyme purification.

### UV-Vis spectroscopic properties of the purified CcO

The reduced spectra of the purified C*c*O from the four samples (Figure 1B) display no appreciable difference in the absorption wavelength of the peaks or the relative intensities between the Soret (445 nm) and alpha heme *a*/$a_3$ (606 nm) absorption peaks. The fact that no peak shift is observed indicates that the coordination states of the heme *a* and heme $a_3$ - $Cu_B$ catalytic centers are not disturbed in the final purified C*c*O by these P+ or P− growth conditions.

### SDS-PAGE analysis of the purified CcO

SDS-PAGE analysis of the four versions of purified C*c*O (Figure 1C) clearly shows that they each contain all of the four subunits, and there is no observable difference between the four samples in terms of subunit composition or the size of the subunits resolvable by the SDS-PAGE. An FPLC peak that eluted earlier than the pure C*c*O contained other respiratory complexes such as a cytochrome $bc_1$ (Complex III) which also appeared unaffected by the P-growth conditions or the CL− mutation (data not shown). Importantly, the combination of phosphate and cardiolipin deficiencies did not cause the C*c*O subunits to dissociate from each other during purification, since the yield of purified enzyme was similar in all cases. This is particularly intriguing with respect to subunit IV, because it is connected to the rest of the enzyme via four phospholipid molecules identified as PE in the four-subunit *R. sphaeroides* C*c*O crystal (22).

### Activity analysis of the purified CcO

The steady state activities (oxygen consumption) of the C*c*O from these four samples are similar (Figure 1D). The addition of soy asolectin, a lipid mixture containing PE, PC, phosphatidylinositol (PI), phosphatidic acid (PA), lysoPC and other unspecified lipids (Avanti Polar Lipids Inc. Alabaster, AL), in the assay increases the activity by 20–30% for all samples, which is typical for purified oxidase produced under normal conditions.

Thus the phosphate-limiting growth condition and the combination of the phosphate-limiting growth and the genetic CL-deficiency do not affect the UV-Vis spectroscopic properties, the subunit composition, the activity of the purified C*c*O enzymes, or the C*c*O expression level (mg C*c*O protein / mg total membrane protein, %: P+ growth, 3.7 ± 1.1%; P− growth, 3.4 ± 0.9%). However, the lipid profiles in the cells are expected to have changed (1). To address the extent and nature of the changes, the lipid profiles in the membrane and in the purified C*c*O enzymes were examined by quantitative ESI and MALDI MS and MS/MS methods with the incorporation of internal lipid standards.

### Membrane lipid analysis by quantitative MS

Figure 2A shows the positive ion mode ESI MS spectra (m/z 600–1000) of the lipids extracted from the resuspended membrane pellets obtained from the four different conditions: WT/ P+, CL−/ P+, WT/ P− and CL−/ P−. Phosphate limitation causes more radical changes in MS lipid profiles than CL limitation alone, as seen for WT/ P+ versus WT/P−, compared to WT/P+ versus CL−/P+. None of the PC and PE lipids predominant in WT/ P+ is observable in WT/ P−, which is now dominated by a new set of lipids. The identities of the lipid species were determined by using MS/MS and $MS^n$ (data not shown). The most abundant ion observed for WT/P− at m/z 764 was determined to be the protonated ion of DGTS (N,N,N-trimethylhomoserine diacylglycerol) 18:1/18:1, a polar non-phospholipid that carries a fixed positive charge in the head group (supplementary Scheme

S1). It also forms a sodium adduct ion at m/z 786, the same m/z as the protonated ion of PC 18:1/18:1, but MS/MS analysis of m/z 786 revealed that it contains only a very low level of PC (product ion m/z 184), and is predominantly the sodium adduct ion of DGTS. Another type of phosphate-free lipid, glucosylgalactosyldiacyllglycerol, GGDG (supplementary Scheme S1), was also observed in the P− growth membranes. Similar drastic lipid profile changes are observed between CL−/ P+ and CL−/ P− in the positive ion mode MS spectra. CL deficiency by itself does not cause such major changes in the lipid species seen in positive ion mode MS (Figure 2A), since the main differences are in levels of cardiolipin itself and other lipids containing negatively charged head groups, which are typically not seen in the positive ion mode.

Figure 2A (panels 3 and 4) shows that in the P− growth, regardless of whether CL is deficient, PC or PE lipid ions do not reach beyond 5% of normalized relative abundance in MS, and DMPE, the intermediate in making PC from PE, also drops to below 5%. In their place, there is an increased level of OL, and the appearance of high levels of DGTS and GGDG lipids. The most abundant fatty acid composition for DGTS is DGTS 18:1/18:1. Correspondingly, the DGTS and GGDG lipids are not detectable in the P+ growth conditions (Figure 2A, panels 1 and 2). Under P+ growth, the CL− mutant has a slightly higher level of PE lipids than the WT wild type, but under P− growth, the CL− mutant does not show an appreciably higher level of OL than WT, although OL has been proposed to be functionally substitutable with PE (1, 3). Both WT and CL− strains show similar high levels of DGTS and GGDG under P− growth, and similar levels of PC under P+ growth.

The negative ion mode ESI MS spectra of the lipids extracted from these four membrane samples are shown in Figure 2B (m/z 600 to 1000). PC and PE are not strongly detected in the negative ion mode MS, but the PG lipids are observed at measurable levels under P+ and P− growth in both the WT and the CL− strains. Appreciable increases in other types of non-phospholipids are also observed. Among these is the peak at m/z 717 in Figure 2B (panels 3 and 4), which is determined to be mainly the glutamine lipid QL 3-OH 20:1/18:1 with a low level of overlapping OL 3-OH 20:1/19:1. This is the first time that the recently discovered glutamine lipid has been found to change under different growth conditions (20, 21). The relative abundance of the SQDG ions also increases in P−.

Results from quantification of the lipid species resolved in negative ion mode MS by using phospholipid internal standards are summarized in Table 1 (with the exception of CL; see below). SQDG, QL and GGDG lipids are relatively quantified by comparison to the PG internal standard, and OL, MMPE and DMPE lipids are relatively quantified by comparing to the PE standard. P− growth causes the PG lipids, including PG 18:1/18:1 and PG 18:0/18:1, to drop by ~50% in both WT and CL− strains. However, PG 18:0/18:0, containing two fully saturated fatty acids and barely observable under P+ growth, increases under P− growth for both WT and CL− strains. P− growth also caused the levels of SQDG lipids, both saturated and unsaturated molecular species, to increase by 2–3 fold for both WT and CL− strains. The QL lipids increased dramatically (over 5 fold) in the P− growth, and the increase of QL 3-OH 20:1/18:1 (m/z 717) is slightly more appreciable in CL− than in WT.

Figure 2C shows the m/z 1200–1600 regions of the negative ion mode ESI MS spectra where singly deprotonated CL ions are detected. In membrane lipid extracts from WT/ P−, cardiolipin only decreases by about 20% compared to its level in WT/ P+, while in CL−/ P+, cardiolipin is already below the ESI MS detection limit. Thus quantification of CL requires CID MS/MS fragmentation at m/z 1455.8 ($CL(18:1)_4$ ) and m/z 1239.5 ($CL(14:0)_4$ internal standard) precursor ions. The results are summarized in Table 1 and Table 2. All of the lipid ions above 5% normalized relative abundance in MS have been quantified by MS/MS in

these samples (Figure 3, Table 1). Since CL is often proposed to be substitutable by PG, and PG has been shown to be functionally exchangeable with SQDG, the quantification of CL (by MS/MS) and PG (by MS), and the relative quantification of SQDG lipids (by MS) are all included in Table 1. The MS/MS quantification of CL clearly indicates that the level of cardiolipin in the CL− mutant was further decreased by the P− growth, and a five-fold "cleaner" CL-deficient membrane sample is obtained through the combination of the CL-deficient mutation with the P− growth (CL−/P−: 0.05 μmol CL/g protein (0.7% of WT/P+); CL−/P+: 0.43 μmol CL/g protein (5.5% of WT/P+) – Table 1, Table 2). Secondly, WT/ P− membranes maintain 73% of the cardiolipin level in WT/ P+. This is in stark contrast to PE and PC, which are found to be nearly completely depleted by the P− growth. These results suggest that in the limited phosphate growth, the highest priority is CL (73% maintained), followed by PG (50% maintained), whereas PE and PC have the lowest priority (Table 2).

While the levels of both PG and CL decrease under P− growth, the non-phospholipid SQDG increases significantly. Since all of the SQDG, PG and CL lipids carry a negative charge and are also capable of forming hydrogen bonds in the head group under physiological conditions, this observation is likely due to the cells' compensatory response in order to maintain the total amount of negative charge at a certain level to meet their physiological needs (2). This suggests that what matters in these lipids is the negatively charged center supplied by carboxylic acid or sulfite groups, usually supplied through phosphate groups. The nearly complete depletion in PC and the concomitant dramatic increase in DGTS, both lipids containing a zwitterionic center carrying a fixed positive charge in the tetra-alkyl amino group, however, suggests that the theme of a zwitterionic center containing a fixed positive charge is also important. The negatively charged phosphate group in PC is replaceable with the carboxylic acid group in DGTS. Since a similar charge center can be provided by the non-phospholipid, the limited phosphate resource is not required to make PC.

Thus in spite of the close-to-wild-type expression and properties of the C*c*O protein in all four conditions, limited phosphate in the growth medium causes drastic changes in the membrane lipid profiles of both the WT and the CL− mutant *R. sphaeroides*. In particular, the combination of the CL− mutation with P− growth creates a significantly more depleted CL-deficient strain than the mutation alone (accompanying paper). The ESI results discussed so far are obtained from the lipid extracts of *R. sphaeroides* membranes in the absence of detergents. For better understanding of the potential role of CL in *R. sphaeroides* C*c*O, it is necessary to look at the lipids that are associated with detergent purified C*c*O, which can be performed more readily using MALDI.

## MALDI analysis of lipids in membranes and purified CcO

Due to the interference from detergents and potential issues associated with incomplete chemical extraction for ESI MS analysis of lipid extracts from the purified C*c*O, direct MALDI MS and MS/MS was applied to perform relative quantification of the lipids in the purified C*c*O, by incorporating a set of internal standards at appropriate concentrations in the enzyme solution. For comparison, the same methods were also applied to direct analysis of the resuspended membrane pellets, and the results were compared to those obtained by ESI on the membrane lipid extracts.

Both MALDI and ESI analyses lead to similar conclusions regarding the relative quantitative changes in the membrane lipids observed as a result of the CL− mutation and/or P− growth. Figure 4A shows the direct MALDI MS spectra of the membranes from the WT/ P+, CL−/ P+, WT/ P− and CL−/ P− *R. sphaeroides* in positive ion mode. Under P− growth (Figure 4A panels 3 and 4), DGTS is the predominant species observed in positive ion mode and PC is nearly completely depleted, consistent with the ESI analysis. Likewise, the

negative ion mode MALDI MS (Figure 4B panels 3 and 4) also reveals the partial retention of PG lipids, and an increase in SQDG (relative to PG internal standard), particularly in the saturated SQDG species, in response to the phosphate depletion in P− growth. The m/z 1200–1600 region of the negative ion mode MALDI MS (Figure 4C) shows that cardiolipin can be detected at 53% in WT/ P− and at 12% in CL−/ P+, compared to WT/ P+ (Table 2), but cannot be detected in CL−/ P−, suggesting CL−/ P− has much less cardiolipin. Also noticeable is that the MALDI MS analysis shows a higher sensitivity for the detection of cardiolipin compared to ESI under the conditions applied here. The comparison of the MALDI MS analysis directly on the membranes with the ESI MS and MS/MS analyses on the membrane lipid extracts shows that the direct MALDI analysis method gives valid quantitative results through incorporating lipid internal standards, optimization of experimental conditions and running multiple replicates of experiments. MALDI is also advantageous in that it is less affected by high levels of detergent in purified enzyme solutions.

Despite the presence of abundant adduct ions unrelated to lipid species (as determined by control experiments), the purified C*c*O from the four different conditions could be analyzed by direct quantitative MALDI MS by comparison with phospholipid internal standards, as shown in Figure 5. In the positive ion mode MS under P+ growth (Figure 5A panels 1 and 2), the phospholipid PC 18:1/18:1 (protonated ions and sodium-adduct ions) is observed as the major lipid species of the purified C*c*O from both WT/ P+ and CL−/ P+. Although known to be present in the purified WT/ P+ C*c*O, PE lipid peaks are not observed likely due to its suppressed ionization efficiency in MALDI in the presence of PC and detergents. Heme *a* from the catalytic center (structure confirmed by MS/MS at m/z 852 and 835) is clearly observed in MS at high ion abundance for all four C*c*O samples. Under P− growth (Figure 5A panels 3 and 4), C*c*O from WT/ P− and CL−/ P− display no detectable PC (m/z 786, 808), while the non-phospholipid DGTS 18:1/18:1 becomes a more abundant lipid ion (m/z 764; identified by MS/MS). The negative ion mode MS spectra show that under P+ growth (Figure 5B panels 1 and 2), PG 18:1/18:1 and a series of SQDG lipids are retained in the purified C*c*O from WT/ P+ and CL−/ P+. By comparison to the PG internal standard at m/z 665, CL−/ P+ C*c*O shows an increased level of PG18:1/18:1 compared to WT/ P+ (m/z 773). However, under P− growth (Figure 5B panels 3 and 4), C*c*O from WT/ P− still contains PG 18:1/18:1 at about 50% of its level in WT/ P+, while in the CL−/ P− sample it decreases and cannot be detected in the MS spectra. SQDG lipids are observed in both of the WT/ P− and the CL− / P− C*c*O samples. These general trends of lipid changes seen in the purified C*c*O are consistent with those seen in the membranes by both ESI (Table 1) and MALDI (Table 2).

The changes in cardiolipin in the four versions of purified C*c*O are shown in the m/z 1200–1600 region of the negative ion mode MALDI MS spectra (Figure 5C). In the WT/ P+ C*c*O (Figure 5C panel 1), several cardiolipin species are detected, including the most abundant CL $(18:1)_4$ at m/z 1455.8 and the less abundant CL $(16:0)_1(18:1)_3$ at m/z 1429.8. A predominant cardiolipin species found in mammalian heart CL $(18:2)_4$ (expected at m/z 1448.8), is notably not present in any of the *R. sphaeroides* C*c*O. The negatively charged sodium or potassium-adducted ions of CL $(18:1)_4$ are also formed at m/z 1478.9 and m/z 1494.9, respectively. The abundant ions at m/z 1495.8 and 1497.8 displayed characteristic fragmentation behaviors in MS/MS and $MS^n$ that are not related to cardiolipin lipids or any known phospholipids. The level of cardiolipin in the purified enzyme from the CL−/ P+ condition is significantly reduced with reference to internal standard CL $(18:1)_4$ : CL $(14:0)_4$ is observable at 27% of the level in WT/ P+ C*c*O. This is higher than the 12% seen in the membrane of CL−/ P+. Under P− growth (Figure 5C panels 3 and 4), the WT/ P− C*c*O still contains about 74% of the cardiolipin level in the WT/ P+ C*c*O, similar to the cardiolipin levels and species in the corresponding membranes. In contrast, the CL−/ P− C*c*O contains

such a low level of cardiolipin that no CL $(18:1)_4$ ions are detectable by MALDI MS, also consistent with the results on the membrane by ESI (Table 1, Table 2).

The results from both the positive and the negative ion mode MALDI MS obtained for WT and CL− C*c*O produced under P+ and P− growth conditions show clearly that in WT/ P− C*c*O, the P-limited growth causes nearly complete depletion of PC and about 50% depletion in PG, but maintains 70% of the level of CL (all percentages are relative to the levels in WT/ P+ C*c*O). Concomitantly, increased levels of the non-phospholipids DGTS and SQDG are seen, similar to the membrane lipid composition changes characterized by ESI. These results demonstrate that when only the P− growth is applied, the WT strain persistently synthesizes and incorporates cardiolipin in C*c*O and cell membranes with a much higher preference over other phospholipids. However, in the P-limited growth combined with the CL− mutation, CL−/ P− C*c*O is depleted of CL to below detectable levels, has lower PG, but increased levels of the non-phospholipid SQDG and an obvious increase in DGTS (m/z 764). These results show that CL−/ P− C*c*O can maintain its native activity and enzyme properties through a mechanism other than selectively enriching CL in the isolated enzyme. With major depletion of CL, PG, and PC, increases of the non-phospholipids DGTS, SQDG and QL, enable C*c*O to remain fully functional. Under abundant supply of phosphate, C*c*O has a preferential specificity for CL lipid, but when CL is not able to be synthesized efficiently, such a preference for CL can be substitutable by PG. When both PG and CL are unavailable, the requirement for CL appears to be successfully replaced by negatively charged non-phospholipids such as SQDG or QL.

## Conclusions

Phosphate-limited growth conditions caused significant selective changes in the lipid profiles of both the *Rhodobacter* membrane and purified cytochrome c oxidase. The bacteria under P− growth conditions display different priorities for making various types of lipids. The first priority is cardiolipin (70% maintained in P−), followed by PG (50% maintained), and the lowest priorities are PE and PC. These latter lipids appear to be successfully substituted by the non-phospholipids DGTS and OL, which contain a similar zwitterionic charge center. QL and SQDG were found to increase by 2–5 fold in the P− growth, suggesting their functional substitution for phospholipids. The fact that purified WT/ P− C*c*O maintains >70% of the CL level found in WT/ P+ C*c*O indicates a significant preference of the bacteria for making CL rather than other phospholipids when phosphate-limited, suggesting that the structural features of CL are more important for the membrane and for C*c*O than PC or PE (even though 6 PE are identified in the *Rs*C*c*O crystal structure (22)). The notable absence of CL containing $(18:2)_4$ in the bacterial system, which is the predominant (and more readily oxidized) form found in mammals (23, 24), may explain the difference in the absolute requirement for this unusual lipid species in diverse organisms.

Phosphate-limited growth combined with the *cls* mutation produced major changes in the lipid profile and a “cleaner” CL− depleted strain, in which the CL levels are reduced to < 1% in the membrane and the purified enzyme, as revealed by both ESI and MALDI. Nevertheless, the resultant purified *R. sphaeroides* C*c*O was remarkably insensitive to the drastically modified lipid content, with regard to subunit composition, spectral properties, enzyme activity, protein expression level and stability during purification.

These findings indicate that the entire structure of CL is not essential for the active form of bacterial C*c*O. The requirement for CL can be fulfilled by PG when available, due to its high structural similarity with respect to negative charge and hydrogen bonding capacity. Further, the requirement for CL and/or PG can also be satisfied by non-phospholipids such as SQDG, and potentially QL, suggesting that the phosphate group can be replaced by negatively

charged sulfite and carboxylic acid groups capable of ionic and hydrogen bond interactions. These observations extend the previous scheme of functional inter-changeability between phospholipids to include non-phospholipids (Table 3).

*In vivo* manipulation of the lipid content of C*c*O by combined metabolic and genetic interventions, coupled with direct MS analysis of the membrane, the purified enzyme and enzyme crystals, provides a powerful tool for further investigating the structural arrangement and dynamic roles of lipids in C*c*O.

## Supplementary Material

Refer to Web version on PubMed Central for supplementary material.

## Abbreviations

| | |
|---|---|
| **R. sphaeroides** | *Rhodobacter sphaeroides* |
| **C*c*O** | cytochrome *c* oxidase |
| ***cls*** | cardiolipin synthase gene |
| **CL** | cardiolipin |
| **PG** | phosphatidylglycerol |
| **PE** | phosphatidylethanolamine |
| **PC** | phosphatidylcholine |
| **OL** | ornithine lipid |
| **QL** | glutamine lipid |
| **SQDG** | sulfoquinovosyldiacylglyceride |
| **CL(+)** | cardiolipin-proficient strain |
| **CL(−)** | cardiolipin-deficient strain |
| **MALDI** | matrix assisted laser desorption/ionization |
| **nESI** | nanoelectrospray ionization |
| **MS** | mass spectrometry |
| **MS/MS** | tandem mass spectrometry |
| **$MS^n$** | multistage tandem mass spectrometry |
| **CID MS/MS** | collision-induced dissociation MS/MS |
| **vMALDI** | vacuum MALDI |
| **MALDI-LIT** | MALDI-linear ion trap |
| **2** | 5-DHB, 2, 5-hydroxybenzoic acid |
| **SDS-PAGE** | sodium dodecyl sulfate polyacrylamide gel electrophoresis |
| **WT** | wild-type |

## References

1. Benning C, Huang ZH, Gage DA. Accumulation of a novel glycolipid and a betaine lipid in cells of *Rhodobacter sphaeroides* grown under phosphate limitation. Arch Biochem Biophys. 1995; 317:103–111. [PubMed: 7872771]

2. Benning C, Beatty JT, Prince RC, Somerville CR. The sulfolipid sulfoquinovosyldiacylglycerol is not required for photosynthetic electron transport in *Rhodobacter sphaeroides* but enhances growth under phosphate limitation. Proc Natl Acad Sci U S A. 1993; 90:1561–1565. [PubMed: 8434018]

3. Lopez-Lara IM, Gao JL, Soto MJ, Solares-Perez A, Weissenmayer B, Sohlenkamp C, Verroios GP, Thomas-Oates J, Geiger O. Phosphorus-free membrane lipids of *Sinorhizobium meliloti* are not required for the symbiosis with alfalfa but contribute to increased cell yields under phosphorus-limiting conditions of growth. Mol Plant-Microbe Interact. 2005; 18:973–982. [PubMed: 16167767]

4. Geiger O, Rohrs V, Weissenmayer B, Finan TM, Thomas-Oates JE. The regulator gene phoB mediates phosphate stress-controlled synthesis of the membrane lipid diacylglyceryl-N,N,N-trimethylhomoserine in *Rhizobium* (*Sinorhizobium*) *meliloti*. Mol Microbiol. 1999; 32:63–73. [PubMed: 10216860]

5. Benning C, Somerville CR. Isolation and genetic complementation of a sulfolipid-deficient mutant of *Rhodobacter sphaeroides*. J Bacteriol. 1992; 174:2352–2360. [PubMed: 1551852]

6. Arondel V, Benning C, Somerville CR. Isolation and functional expression in *Escherichia coli* of a gene encoding phosphatidylethanolamine methyltransferase (EC 2.1.1.17) from *Rhodobacter sphaeroides*. J Biol Chem. 1993; 268:16002–16008. [PubMed: 8340421]

7. Benning C. Biosynthesis and function of the sulfolipid sulfoquinovosyl diacylglycerol. Annu Rev Plant Physiol Plant Mol Biol. 1998; 49:53–75. [PubMed: 15012227]

8. Tamot, B. MSthesis. Department of Biochemistry & Molecular Biology. Michigan State University; 2006. Construction and characterization of a cardiolipin-deficient mutant in *Rhodobacter sphaeroides*.

9. Chang SC, Heacock PN, Mileykovskaya E, Voelker DR, Dowhan W. Isolation and characterization of the gene (CLS1) encoding cardiolipin synthase in Saccharomyces cerevisiae. J Biol Chem. 1998; 273:14933–14941. [PubMed: 9614098]

10. Xie J, Bogdanov M, Heacock P, Dowhan W. Phosphatidylethanolamine and monoglucosyldiacylglycerol are interchangeable in supporting topogenesis and function of the polytopic membrane protein lactose permease. J Biol Chem. 2006; 281:19172–19178. [PubMed: 16698795]

11. Sistrom WR. A requirement for sodium in the growth of *Rhodopseudomonas spheroides*. J Gen Microbiol. 1960; 22:778–785. [PubMed: 14447230]

12. Sistrom WR. The kinetics of the synthesis of photopigments in *Rhodopseudomonas spheroides*. J Gen Microbiol. 1962; 28:607–616. [PubMed: 13913485]

13. Zhen Y, Qian J, Follmann K, Hayward T, Nilsson T, Dahn M, Hilmi Y, Hamer AG, Hosler JP, Ferguson-Miller S. Overexpression and purification of cytochrome c oxidase from Rhodobacter sphaeroides. Protein Expression Purif. 1998; 13:326–336.

14. Qin L, Hiser C, Mulichak A, Garavito RM, Ferguson-Miller S. Identification of conserved lipid/detergent-binding sites in a high-resolution structure of the membrane protein cytochrome c oxidase. Proc Natl Acad Sci U S A. 2006; 103:16117–16122. [PubMed: 17050688]

15. Hiser C, Mills DA, Schall M, Ferguson-Miller S. C-Terminal truncation and Histidine-tagging of cytochrome *c* oxidase subunit II reveals the native processing site, shows involvement of the C-terminus in cytochrome *c* binding, and improves the assay for proton pumping. Biochemistry. 2001; 40:1606–1615. [PubMed: 11327819]

16. Hosler JP, Fetter J, Tecklenburg MMJ, Espe M, Lerma C, Ferguson-Miller S. Cytochrome *aa3* of *Rhodobacter sphaeroides* as a model for mitochondrial cytochrome *c*-oxidase. Purification, kinetics, proton pumping, and spectral analysis. J Biol Chem. 1992; 267:24264–24272. [PubMed: 1332949]

17. Awasthi YC, Chuang TF, Keenan TW, Crane FL. Tightly bound cardiolipin in cytochrome oxidase. Biochim Biophys Acta. 1971; 226:42–52. [PubMed: 4323697]

18. Zhang X, Reid GE. Multistage tandem mass spectrometry of anionic phosphatidylcholine lipid adducts reveals novel dissociation pathways. Int J Mass Spectrom. 2006; 252:242–255.

19. Gage DA, Huang ZH, Benning C. Comparison of sulfoquinovosyl diacylglycerol from spinach and the purple bacterium *Rhodobacter sphaeroides* by fast atom bombardment tandem mass spectrometry. Lipids. 1992; 27:632–636. [PubMed: 1406075]

20. Zhang X, Ferguson-Miller SM, Reid GE. Characterization of ornithine and glutamine lipids extracted from cell membranes of *Rhodobacter sphaeroides*. J Am Soc Mass Spectrom. 2009; 20:198–212. [PubMed: 18835523]

21. Zhang, X. PhD thesis. Department of Chemistry and Department of Biochemistry & Molecular Biology. Michigan State University; 2009. Investigating the Functional Roles of Lipids in Membrane Protein Cytochrome *c* Oxidase from *Rhodobacter sphaeroides* Using Mass Spectrometry and Lipid Profile Modification.

22. Svensson-Ek M, Abramson J, Larsson G, Tornroth S, Brzezinski P, Iwata S. The x-ray crystal structures of wild-type and EQ(I-286) mutant cytochrome *c* oxidases from *Rhodobacter sphaeroides*. J Mol Biol. 2002; 321:329–339. [PubMed: 12144789]

23. Chicco AJ, Sparagna GC. Role of cardiolipin alterations in mitochondrial dysfunction and disease. Am J Physiol. 2007; 292:C33–C44.

24. Xu Y, Malhotra A, Ren M, Schlame M. The enzymatic function of tafazzin. J Biol Chem. 2006; 281:39217–39224. [PubMed: 17082194]

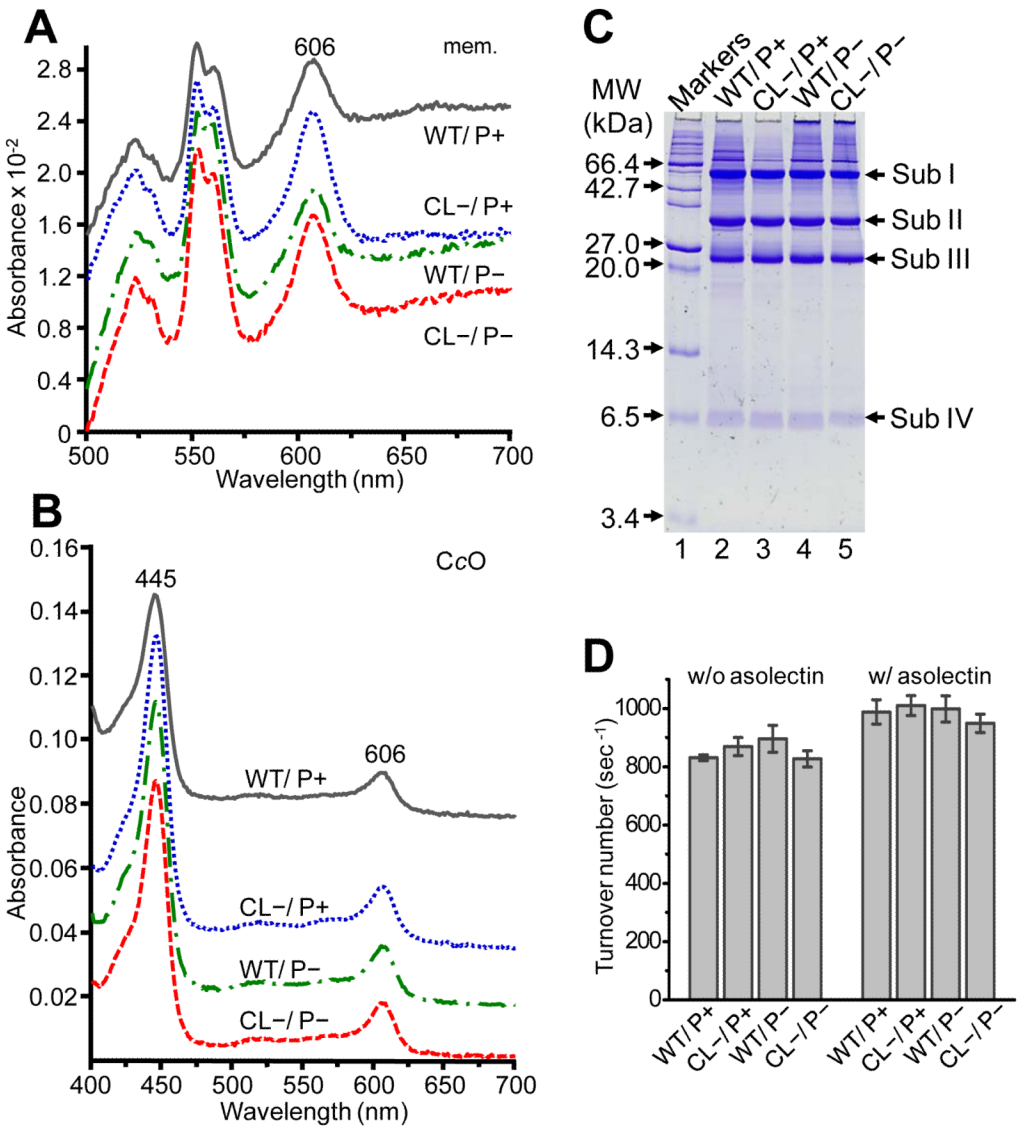


**Figure 1.**

Expression and activity of C*c*O from *R. sphaeroides*. (A) Reduced minus oxidized UV-Vis spectra of the resuspended membranes from the four different conditions showing the native spectral band at 606 nm and the high level of expression (peak height at 606 nm vs 560 nm). (B) Absolute spectra of C*c*O purified from these membranes by $Ni^{2+}$-NTA FPLC showing the identical peak positions at 445 nm and 606 nm indicating that the purified C*c*Os all have native spectral characteristics. (C) SDS-PAGE of purified C*c*O showing the four subunits normally seen in *Rs*C*c*O. The fainter molecular weight bands above the major band of subunit I are a polymerization artifact that occurs during the sample preparation for the SDS gel. (D) Steady-state oxygen consumption activity analysis of the purified C*c*Os measured in 30 μM cytochrome *c*, 1 mM TMPD, 2.8 mM ascorbic acid, 0.05 % dodecyl maltoside in 50 mM $KH_2PO_4$ (pH 6.5) buffer with and without asolectin lipids (1.1 mg/mL final concentration of soybean asolectin and 0.02% (m/v) final concentration of cholate). Gray = WT/ P+; Blue = CL−/ P+; Green = WT/ P−; and Red = CL−/ P−. None of the enzymes alone (nor cytochrome *c* alone) had a significant oxidation rate in the assay buffer system, indicating a specific cytochrome *c* oxidase reaction.

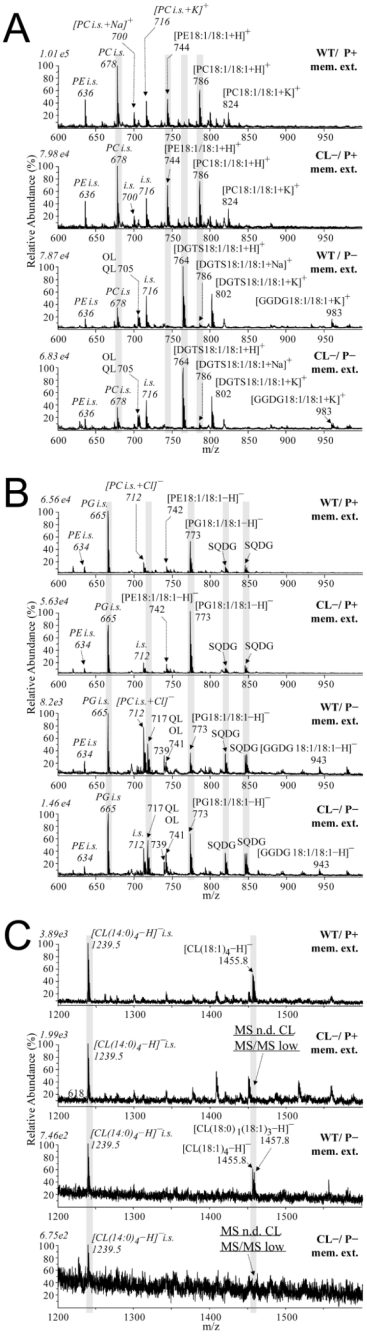


**Figure 2.**

ESI MS spectra of membrane extracts (mem. ext.) from the same amount of isolated membranes of *R. sphaeroides* strains WT/ P+, CL−/ P+, WT/ P− and CL−/ P− prepared as described in Methods. The data show the marked changes in lipid species in response to the *cls*-mutation and the phosphate-limited growth conditions. Species that show alterations are highlighted, in particular the loss of CL at m/z 1455.8 in CL-P- membranes. (A) positive ion mode, (B) negative ion mode, m/z 600–1000, and (C) negative ion mode, m/z 1200–1600. Phospholipid internal standards are labeled as i.s. and include PE (m/z 636), PC (m/z 678) in positive ion mode (A); PE (m/z 634), PG (m/z 665), PC+Cl (m/z 712) in negative ion mode (B); and CL (m/z 1239.5) in negative ion mode(C). The % relative abundance scale shows

numbers above the Y-axis that give the absolute abundance of the most abundant peak to which the other peaks are scaled; e.g. 1.01e5, indicates the absolute ion count of the most abundant peak (PC i.s. m/z 678) is 10,100. The data is quantified on the basis of relative peak heights compared to internal standards. The results of the quantification are summarized in Fig 3 and in Tables 1 and 2.

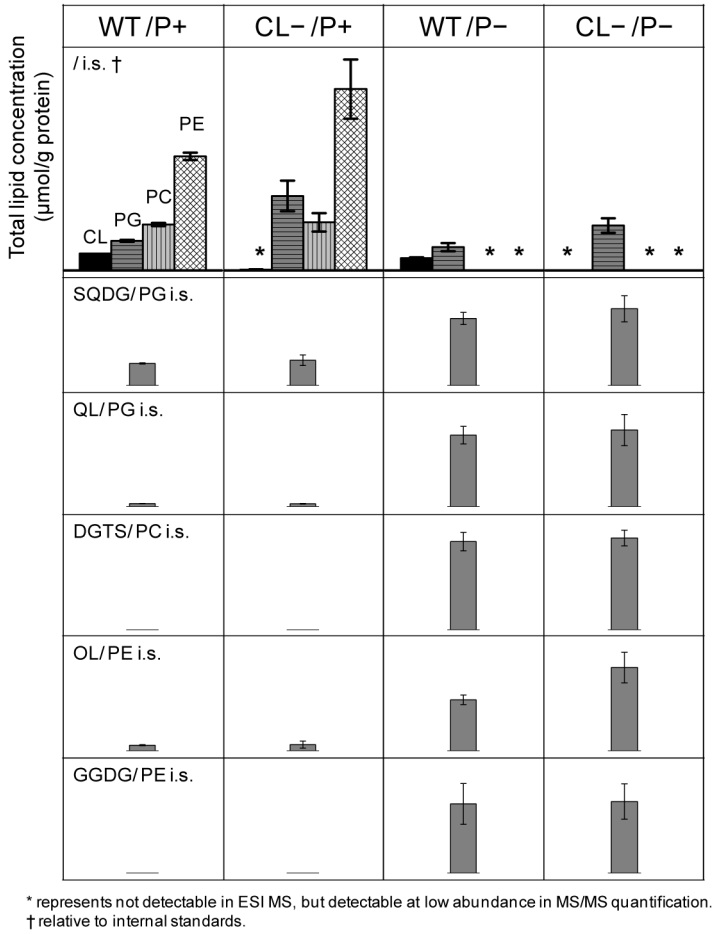


**Figure 3.**

Summary of quantification of the membrane lipids in WT/ P+, CL−/ P+, WT/ P− and CL−/ P− using ESI MS following lipid extraction. The total content of each lipid in μmol/g protein is calculated on the basis of known amounts of internal standards for CL, PG, PC and PE, and known amounts of protein, as described in Materials and Methods. Where no standard is available, the closest related chemical structure was used to give a relative change in SQDG, QL, DGTS, OL, and GGDG. These non-phospholipids all showed significant apparent increases compared to the diminished levels of the phospholipids under P− growth. More detailed analysis of the lipid species is presented in Table 1.

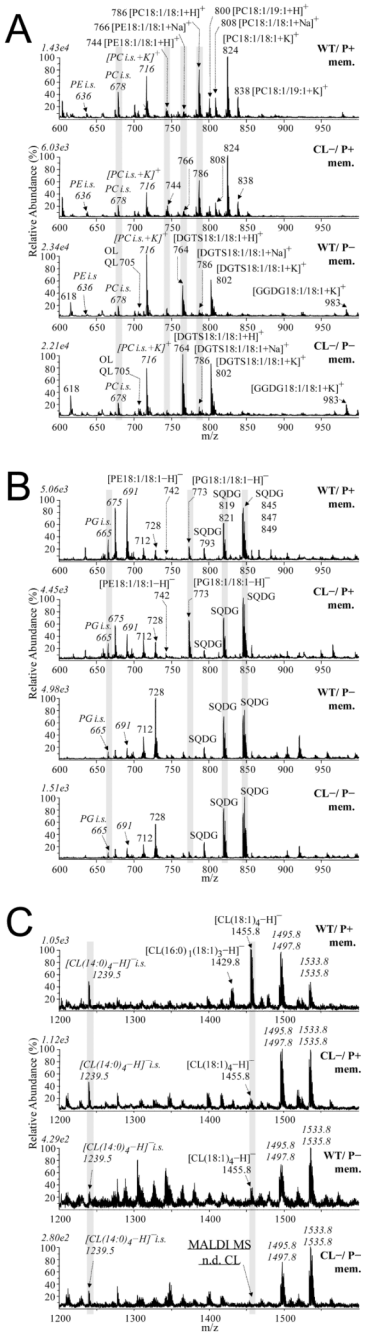


**Figure 4.**

Direct MALDI MS quantification of lipids relative to phospholipid internal standards (i.s.) in the unextracted isolated membranes (mem.) from *R. sphaeroides* strains under different growth conditions as described in Materials and Methods: WT/ P+, CL−/ P+, WT/ P− and CL−/ P−. (A) positive ion mode, (B) negative ion mode m/z 600–1000, and (C) negative ion mode m/z 1200–1600. The highlighted peaks emphasize internal standards and lipids of interest. In (A) under P− conditions loss of PC (m/z 286, 824, 838) and gain of DGTS (m/z 802) is seen, while in (B) under P− conditions, there is relative loss of PG (m/z 773) and retention of SQDG (m/z 819,821,845, 847 849). In (C) under P− conditions, loss of CL (m/z 1455.8, 1429.8) is seen relative to CL internal standard (m/z 1239.5). The negative ion mode

peaks at m/z 1495.9, 1497.9, 1533.8 and 1535.8 were determined by MS/MS and $MS^n$ not to be CL or CL derivatives.

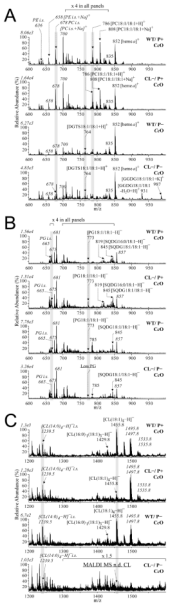

**Figure 5.**

Direct MALDI MS analysis of lipids in the unextracted C*c*O purified from *R. sphaeroides* strains WT/ P+, CL−/ P+, WT/ P− and CL−/ P−. Phospholipid internal standards (i.s.) allows for quantification of the lipid species. The strains and different growth conditions are described in Materials and Methods. (A) positive ion mode, (B) negative ion mode m/z 600–1000, and (C) negative ion mode m/z 1200–1600. As in Figure 4, m/z peaks of internal standards and lipids of particular interest are highlighted. In (A) under P− conditions, loss of PC (m/z 786, 808) but increased DGTS (764) is indicated. In (B) under P− conditions, loss of PG but retention of SQDG (m/z 845) is seen. In (C) bottom panel, the P− conditions combined with the CL(−) mutant result in major loss of CL (m/z 1455.8). These results are summarized in Table 2.

**Table 1**

Quantification of membrane lipids using ESI MS and MS/MS

| lipid type | lipid species\strain | WT/P+ | CL−/P+ | WT/P− | CL−/P− | method |
|---|---|---|---|---|---|---|
| **CL** | CL 18:1 | 7.69±n/a | 0.43±0.09 | 5.64±0.36 | 0.05±0.00 | **Absolute** |
| **PG** | PG 18:1/18:1 | 10.9±0.3 | 28.3±5.9 | 6.9±0.6 | 14.6±2.3 | |
| | PG 18:0/18:1 | 2.0±0.0 | 4.3±0.9 | 1.9±0.4 | 4.1±0.9 | |
| | PG 18:0/18:0 | 0 | 0.3±0.0 | 0.7±0.3 | 0.8±0.1 | |
| | PG 18:1/19:1 | 0.5±0.0 | 0.9±0.2 | 1.1±0.6 | 0.9±0.1 | |
| **PE** | PE 18:1/18:1 | 44.0±1.4 | 71.1±11.1 | 0 | 0 | |
| | PE 18:0/18:1 | 7.8±0.3 | 11.1±2.4 | 0 | 0 | |
| **PC** | PC 16:0/18:0 | 1.2±0.1 | 1.1±0.2 | 0 | 0 | |
| | PC 18:1/18:1 | 13.3±0.3 | 15.4±2.8 | 0 | 0 | |
| | PC 18:0/18:1 | 1.4±0.2 | 1.6±0.5 | 0 | 0 | |
| | PC 18:1/19:1 | 4.9±0.2 | 3.7±0.7 | 0 | 0 | |
| **SQDG** | SQDG 16:0/16:0 | 0.8±0.0 | 0.5±0.1 | 2.3±0.3 | 2.8±0.4 | **Relative** |
| | SQDG 16:0/18:1 | 2.2±0.1 | 2.3±0.6 | 7.4±0.6 | 8.0±1.1 | |
| | SQDG 16:0/18:0 | 1.1±0.1 | 1.1±0.1 | 2.6±0.4 | 3.4±0.7 | |
| | SQDG 18:1/18:1 | 2.9±0.1 | 3.6±0.9 | 7.3±0.6 | 8.1±1.2 | |
| | SQDG 18:0/18:1 | 1.4±0.0 | 2.0±0.4 | 5.9±0.3 | 6.7±1.3 | |
| | SQDG 18:0/18:0 | 0.3±0.0 | 0.3±0.0 | 0.8±0.3 | 1.1±0.5 | |
| **OL** | OL 3-OH 18:0/19:1 | 0 | 0 | 0 | 27.6±1.9 | |
| | OL 3-OH 18:1/20:2, OL 3-OH 18:0/20:3 | 0 | 0 | 0 | 27.5±n/a | |
| | OL 3-OH 20:1/18:1 | 4.0±n/a | 2.4±6.0 | 53.6±6.3 | 66.8±15.3 | |
| | OL 3-OH 20:0/18:1, OL 3-OH 20:1/18:0 | 0 | 0 | 46.1±4.6 | 56.5±13.4 | |
| | OL 3-OH 20:1/19:1 | 8.5±1.3 | 11.0±2.2 | 25.6±1.0 | 26.1±6.9 | |
| | OL 3-OH 20:0/21:1 | 1.0±0.0 | 1.7±0.4 | 0 | 0 | |
| **QL** | QL 3-OH 20:1/18:1 mainly, OL 3-OH 20:1/19:1 | 0.7±0.1 | 0.7±0.1 | 11.8±1.6 | 12.3±2.4 | |
| | QL 3-OH 20:0/18:1 mainly | 0 | 0 | 5.8±0.5 | 6.5±1.4 | |
| **DGTS** | DGTS 18:1/18:1 | 0 | 0 | 63.0±6.9 | 66.0±5.7 | |
| | DGTS 18:0/18:1 | 0 | 0 | 23.5±2.2 | 24.1±2.0 | |

| lipid type | lipid species\strain | WT/P+ | CL−/P+ | WT/P− | CL−/P− | method |
|---|---|---|---|---|---|---|
| **GGDG** | GGDG18:1/18:1+K | 0 | 0 | 27.4±8.1 | 28.3±7.0 | |
| **MMPE, DMPE, PE** | MMPE 18:1/18:1, PE 19:1/18:1, PE 18:1/19:1 | 7.9±0.5 | 8.8±n/a | 8.3±n/a | 8.5±n/a | |
| | MMPE 18:1/19:1, MMPE 19:1/18:1, DMPE 18:1/18:1, PE 18:1/20:1, PE 20:1/18:1 | 12.0±4.6 | 9.9±2.4 | 0 | 0 | |
| | DMPE 18:1/18:1 | 10.6±0.9 | 16.7±4.9 | 0 | 0 | |

Keys:

1. The quantities of lipids are represented as μmol of lipids/ g membrane protein.
2. The phopholipids CL, PG, PE and PC are represented as absolute quantities, and the other lipids without internal standards are quantified with respect to the most related internal standards (OL, MMPE, DMPE and GGDG/PE i.s., QL/PG i.s., SQDG/PG i.s. and DGTS/PC i.s.) for relative comparisons following isotopic corrections.
3. Values represent the means ± systematic errors calculated from standard deviation of at least three independent extractions. n/a indicates error not available.

## Table 2

Comparison of ESI and MALDI analysis of CL content in the membrane and purified C*c*O of the P+ and P− growths of WT and CL−

| | sample | membrane | C*c*O |
|---|---|---|---|
| ESI | WT/ P+ | 100%* | n/a |
| MS/MS | CL−/ P+ | 5.5±1.1% | n/a |
| | WT/ P− | 73.3±4.7% | n/a |
| | CL−/ P− | 0.7±0% | n/a |
| MALDI | WT/ P+ | 100%† | 100%^ |
| | CL−/ P+ | 12±4% | 27±3% |
| | WT/ P− | 53±18% | 74±14% |
| | CL−/ P− | MS n/d | MS n/d |

*100% represents absolute value 7 μmol lipid /g membrane protein (see Table 1).

†100% represents 12.5μmol lipid /g membrane protein relative to single internal standard.

^100% represents 5.3 μmol lipid / g C*c*O protein.

n/d= not detected; n/a= not available.

**Table 3**

Possible functional interchangeability between different types of membrane and C*c*O lipids in *R. sphaeroides in vivo*

| Head group charge | Non-PL | Phospholipids (PL) |
|---|---|---|
| Negative | QL | ***Cardiolipin*** |
| | SQDG ⟷ | Phosphatidylglycerol |
| Zwitterionic: fixed | DGTS ⟷ | Phosphatidylcholine |
| Zwitterionic: mobile | OL ⟷ | Phosphatidylethanolamine |
| Neutral | GGDG | |